Modeling Backscatter Properties of Snowfall at Millimeter Wavelengths

SERGEY Y. MATROSOV

Cooperative Institute for Research in Environmental Sciences, University of Colorado, and NOAA/Earth System Research Laboratory, Boulder, Colorado

(Manuscript received 26 April 2006, in final form 20 July 2006)

ABSTRACT

Ground-based vertically pointing and airborne/spaceborne nadir-pointing millimeter-wavelength radars are being increasingly used worldwide. Though such radars are primarily designed for cloud remote sensing, they can also be used for precipitation measurements including snowfall estimates. In this study, modeling of snowfall radar properties is performed for the common frequencies of millimeter-wavelength radars such as those used by the U.S. Department of Energy's Atmospheric Radiation Measurement Program (K_a and W bands) and the CloudSat mission (W band). Realistic snowflake models including aggregates and single dendrite crystals were used. The model input included appropriate mass–size and terminal fall velocity–size relations and snowflake orientation and shape assumptions. It was shown that unlike in the Rayleigh scattering regime, which is often applicable for longer radar wavelengths, the spherical model does not generally satisfactorily describe scattering of larger snowflakes at millimeter wavelengths. This is especially true when, due to aerodynamic forcing, these snowflakes are oriented primarily with their major dimensions in the horizontal plane and the zenith/nadir radar pointing geometry is used. As a result of modeling using the experimental snowflake size distributions, radar reflectivity–liquid equivalent snowfall rates (Z_e–S) relations are suggested for "dry" snowfalls that consist of mostly unrimed snowflakes containing negligible amounts of liquid water. Owing to uncertainties in the model assumptions, these relations, which are derived for the common K_a- and W-band radar frequencies, have significant variability in their coefficients that can exceed a factor of 2 or so. Modeling snowfall attenuation suggests that the attenuation effects in "dry" snowfall can be neglected at the K_a band for most practical cases, while at the W band attenuation may need to be accounted for in heavier snowfalls observed at longer ranges.

1. Introduction

Traditional radar methods of measuring precipitation are based on relations between water equivalent reflectivity factor (hereafter "reflectivity"), Z_e, and precipitation rate, R. Even for a simpler case of rainfall, there are significant variations in Z_e–R relations due to variability of the drop size distributions. Estimating snowfall parameters from radar measurements is more challenging. Variability in snowflake shapes, densities, and fall velocities results in greater uncertainties in Z_e–R relations for snowfall. Notwithstanding these uncertainties, radar gives an opportunity to obtain near-real-time estimates of snowfall rate and accumulation, providing information that is not readily available with other remote sensors.

As for rainfall, snowfall radar estimates are typically obtained with longer wavelength (centimeter) radars such as those that operate at S band (10–11-cm wavelength, λ), C band ($\lambda \sim 5$–6 cm), or X band ($\lambda \sim 3$ cm). Snowfall rate as inferred from radar measurements is usually expressed in melted liquid equivalent, S, rather than in solid snow rate. Two different approaches are used to derive Z_e–S relations. In one approach both Z_e and S are calculated from theoretical or experimental snowflake size distributions (SSD) and they are related in a statistical manner (e.g., Sekhon and Srivastava 1970; Matrosov 1992). In the second approach, radar measurements of reflectivity are related to the snowfall rate as observed by nearby snow gauges (e.g., Super and Holroyd 1998; Hunter and Holroyd 2002). Rasmussen et al. (2003) provides a review of some Z_e–S relations suggested for use with longer-wavelength radars. For such radars, snowflakes are typically much smaller than radar wavelength and scattering does not deviate significantly from the Rayleigh law.

Corresponding author address: Dr. Sergey Matrosov, R/PSD2, 325 Broadway, Boulder, CO 80305.
E-mail: Sergey.Matrosov@noaa.gov

DOI: 10.1175/JAS3904.1

At millimeter radar wavelengths such as those at K_a band ($\lambda \sim 8$ mm) and, especially, W band ($\lambda \sim 3$ mm), scattering by typical snowflakes is generally non-Rayleigh. Radars operating at these wavelengths have been primarily intended for applications in cloud remote sensing and they have typically not been used for snowfall measurements. It has been shown, however, that the use of such radars in pair with centimeter-wavelength radars can potentially improve the accuracy of snowfall parameter retrievals (Matrosov 1998; Liao et al. 2005; Wang et al. 2005) because the dual wavelength reflectivity ratio provides independent information on characteristic size of snowflakes. Knowing size information, one can better infer snowfall rate from single reflectivity measurements.

Currently, a number of vertically pointing millimeter-wavelength radars operate on a continuing basis in many locations including those that regularly or sometimes get snowfalls. Examples of such radars are vertically pointing K_a-band (34.6 GHz) millimeter-wavelength cloud radars (MMCR) operated by the U.S. Department of Energy's Atmospheric Radiation Measurement Program (DOE ARM) in Oklahoma and the North Slope of Alaska (NSA). Another MMCR-type radar has been recently deployed in the Canadian Arctic. The W-band (94 GHz) nadir-looking CloudSat radar will provide global information on reflectivity profiles of hydrometeors (Stephens et al. 2002). Although the main objective of all these radars is cloud remote sensing, their measurements of snowfall can also be interpreted quantitatively, thus providing valuable information on snowfall accumulation and the vertical structure of snowfall rate, which can vary significantly (Mitchell 1988).

Since for most of the radars mentioned above there are no collocated centimeter-wavelength radars for application of dual-wavelength ratio techniques, Z_e–S relations specifically tailored for millimeter wavelengths are needed for quantitative interpretation of snowfall measurements. This article presents results of modeling Z_e–S relations for the common millimeter-wavelength frequencies of 34.6 and 94 GHz based on available information on snowflake-size distributions and densities. The first of the aforementioned approaches for deriving Z_e–S relations is employed here because there are no reliable datasets available that combine collocated millimeter-wavelength radar and snow gauge measurements. This modeling is concerned with so called "dry" snow, the term usually used for describing snow with negligible amounts of liquid water/riming. "Dry" snowfalls usually contribute most significantly to snow accumulation at temperatures less than about −8°C.

2. Snowflake model

a. Snowflake shape

The Rayleigh scattering conditions at a radar wavelength λ for a snow particle with a major dimension D can be formulated as follows:

$$x = \pi D/\lambda \ll 1, \tag{1}$$

$$\pi D|m_s|/\lambda \ll 1, \tag{2}$$

where m_s is the complex refractive index of snow. The great majority of derivations of Z_e–S relations in snowfall assumed that for snowflakes that satisfy these conditions the radar backscatter would be the same as that of a sphere of solid ice having the same mass. While this assumption precludes modeling polarimetric properties of backscatter cross sections, it provides a reasonably good approximation of Z_e for low-density dry snow at centimeter wavelengths. The spherical model, however, becomes progressively less suitable as the size parameter x increases beyond the bounds of the Rayleigh conditions. Larger nonspherical ice particles exhibit backscatter dependence on particle orientation (e.g., Matrosov 1993; Aydin and Singh 2004) and generally greater reflectivities (especially outside the Rayleigh scattering regime) compared to those of spherical particles of the same mass (Matrosov et al. 2005a).

The simplest geometrical shape that allows describing nonspherical hydrometeors is that of spheroid. In their classical observational in situ study, Magono and Nakamura (1965) used tracing outlines of snowflakes that revealed a generally spheroidal shape. The oblate spheroidal model is used widely in the radar community to model raindrops and it was also shown to satisfactorily describe and explain depolarization observations of snowflakes at K_a band (Matrosov et al. 1996, 2001). Note also that, at radar frequencies, the small details in a particle structure usually do not significantly affect the backscatter properties that depend largely on the overall shape (Dungey and Bohren 1993), which, in the case of spheroid, is determined by the spheroid aspect ratio, r. This is especially true for smaller snowflake size parameters $x = \pi D\lambda^{-1}$ (Schneider and Stephens 1995). The applicability of the spheroid model for larger snowflakes with small values of r (e.g., dendrites that are larger than several millimeters) at W band is not so obvious. This model, however, satisfactorily explains experimental 94-GHz aggregate snow reflectivities (Matrosov et al. 2005a).

Based on the arguments given above, and also due to the fact that very large dendrites are not very common, the oblate spheroidal model was adopted here for snowflake modeling. Another reason to use this model

is the lack of detailed shape information on aggregates, which makes the input information for the computational models that are able to account for fine shape details (e.g., the discrete dipole approximation; Lemke and Quante 1999) not very well defined. In the spheroid model, low aspect ratio values of about 0.1–0.3 are suitable for modeling pristine dendrite snow crystals, while values of $r \approx 0.5$–0.7 are usually observed for larger aggregate crystals (Magono and Nakamura 1965; Korolev and Isaac 2003). The value around $r \approx 0.6$ also best explains experimental dual-wavelength ratios from the airborne radars operating at 9.6 and 94 GHz (Matrosov et al. 2005a).

b. Snowflake orientation

Magono and Nakamura (1965) noted that, due to aerodynamic forcing, snowflakes typically fall with their major dimensions oriented horizontally. Polarimetric radar depolarization measurements at different polarimetric bases and at different elevation angles also reveal that, in the absence of strong horizontal winds (and wind shear), single shape snowflakes are oriented preferably horizontally with a standard deviation (SD) of about 9° (Matrosov et al. 2005b). Thus it was assumed during modeling that symmetry axes of oblate spheroids that approximate snowflakes are oriented with the 0° mean and SD = 9° with respect to vertical. While there is no polarization dependence of radar measurables for vertically pointing radar for such snowflake orientations, snowflake shape and, to a lesser extent, the value of SD influence the magnitude of Z_e at millimeter-wavelength frequencies.

c. Snowflake mass

According to Magono and Nakamura (1965), density, ρ, of falling dry aggregate snowflakes that are larger than 0.2 cm diminishes with their size from approximately 0.03 g cm^{-3} at $D = 0.2$ cm to about 0.01 g cm^{-3} at $D = 1.5$ cm. While $D \approx 0.2$ cm is the smallest size presented by Magono and Nakamura (1965), there are a number of microphysical studies in which ice aggregates with sizes less than 0.2 cm were studied (e.g., Brown and Francis 1995; Mitchell 1996; Heymsfield et al. 2004). Most of these studies indicate that the mass, m, of an aggregate particle typically increases as D^b, where $b \approx 2$. The following formulas provide a continuous mass–size relation for snowflakes for a large range of possible sizes:

$$m\,(\mathrm{g}) = 0.003D^2 \quad (0.01\ \mathrm{cm} < D \le 0.2\ \mathrm{cm}), \tag{3a}$$

$$m\,(\mathrm{g}) = 0.0067D^{2.5} \quad (0.2\ \mathrm{cm} < D \le 2.0\ \mathrm{cm}), \tag{3b}$$

$$m\,(\mathrm{g}) = 0.0047D^3 \quad (D > 2\ \mathrm{cm}). \tag{3c}$$

A lower limit of $D = 0.01$ cm was chosen in (3a) because for smaller sizes this formula can provide results that correspond to unrealistic densities exceeding those of solid ice. While (3b) closely approximates data from Magono and Nakamura (1965), (3a) provides particle masses that are within the range of empirical relations of the aforementioned studies for smaller aggregate particles. Note that (3a) is very close to the relation for aggregates S3 (according to the Magono and Lee 1966 classification) suggested by Mitchell (1996):

$$m = 0.0028D^{2.1}\ (\mathrm{cgs\ units}), \tag{4}$$

and is also in good agreement with later findings by Mitchell and Heymsfield (2005).

Equation (3c) reflects the fact that the density of very large snowflakes does not exhibit any significant dependence on size.

In addition to aggregate snowflakes, modeling was also performed for single dendrite snowflakes. While snowfalls consisting of single dendrites typically do not yield significant accumulations on the ground, such modeling was performed in order to better understand the generality of the derived Z_e–S relations. According to Heymsfield (1972) density–size relations for dendrites (P1e according to the Magono and Lee classification) and stellars with broad arms (P1d) are practically identical. For such crystals Mitchell (1996) suggests the following relation:

$$m\,(\mathrm{g}) = 0.000\,27D^{1.67} \quad (0.009\ \mathrm{cm} < D \le 0.15\ \mathrm{cm}), \tag{5}$$

which was used for modeling of dentritic crystals in this study.

d. Snowflake fall velocity

Terminal fall velocities of hydrometeors, v_t, are determined by their mass, their area projected to the flow, their size, and such air properties as density ρ, and dynamic viscosity η. In a recent study, Mitchell and Heymsfield (2005) critically addressed existing fall velocity–size relations for aggregate ice crystals. They suggested a refined relation that accounts for the correspondence between the Reynolds and the Best or Davies numbers that is appropriate for aggregates. The data presented by Mitchell and Heymsfield (2005, their Fig. 5) indicate an approximately linear relation between v_t and the logarithm of aggregate size. This linear relation can be expressed as

$$v_t\,(\mathrm{cm\ s^{-1}}) \approx 30 + 50[\log_{10}(D) - 2]\ (\mathrm{for}\ D > 100\ \mu\mathrm{m}), \tag{6}$$

where D is in microns. For 0.16 cm $< D <$ 1 cm, expression (6) also approximates well the measurement-derived fall velocity relation for large unrimed aggregates of dendritic crystals suggested by Locatelli and Hobbs (1974).

Many theoretical (e.g., Mitchell and Heymsfield 2005) and experimental (e.g., Magono and Nakamura 1965) studies indicate that terminal fall velocities of larger snowflakes practically do not depend upon the size of the flake. Taking this into consideration, it was assumed that (6) describes aggregate snowflake fall velocities in the range 0.01 cm $< D <$ 1 cm and the constant value of v_t was then assumed for $D \geq 1$ cm.

For single dentritic snowflakes (P1d), the fall velocity–size relation can be approximated as

$$v_t = 75D^{0.3} \text{ (P1d, } D < 0.15 \text{ cm, cgs units)}, \quad (7)$$

which is in general agreement with the Heymsfield (1972), Mitchell (1996), and Mitchell and Heymsfield (2005) data. Terminal fall velocities aloft at an altitude h can be calculated from those at the surface using the expression (Pruppacher and Klett 1997)

$$v_t(\text{h}) = v_t(0)[\rho(\text{h})/\rho(0)]^{\alpha-1}/[\eta(\text{h})/\eta(0)]^{1-2\alpha}, \quad (8)$$

where η and ρ are the air dynamic viscosity and density [$\rho(0) = 1.23$ kg m^{-3}, $\eta(0) = 1.65 \times 10^{-5}$ Pa s], respectively, and $\alpha = 0.57$ for snowflakes. It should be noted that the fall velocity approximations considered above are applicable to snowflakes with a negligible degree of riming. Rimed and wet snowflakes and also graupel generally exhibit higher fall velocities. Snowfalls consisting of such particles are usually observed at temperatures near freezing and when significant amounts of supercooled water drops are present in the atmosphere. This study focuses on "dry" snow.

3. Backscatter cross sections of individual snowflakes

The T-matrix method (Barber and Yeh 1975) was used for calculations of snowflake scattering properties. Input parameters for the T-matrix code include snowflake size, aspect ratio, complex refractive index and the direction of the incident radar beam. A snowflake is considered a uniform mixture of solid ice and air where solid ice details that are typically much smaller than the radar wavelength are ignored. Based on the mass and volume of a snowflake, its effective density is calculated and the relative volumes of solid ice (P_i) and air (P_a) are computed. The complex refractive index of a bulk snowflake mixture, m_s, is then calculated using the approach that is often used in modeling dielectric properties of dry snow at radar frequencies (e.g., Battan 1973; Oguchi 1983):

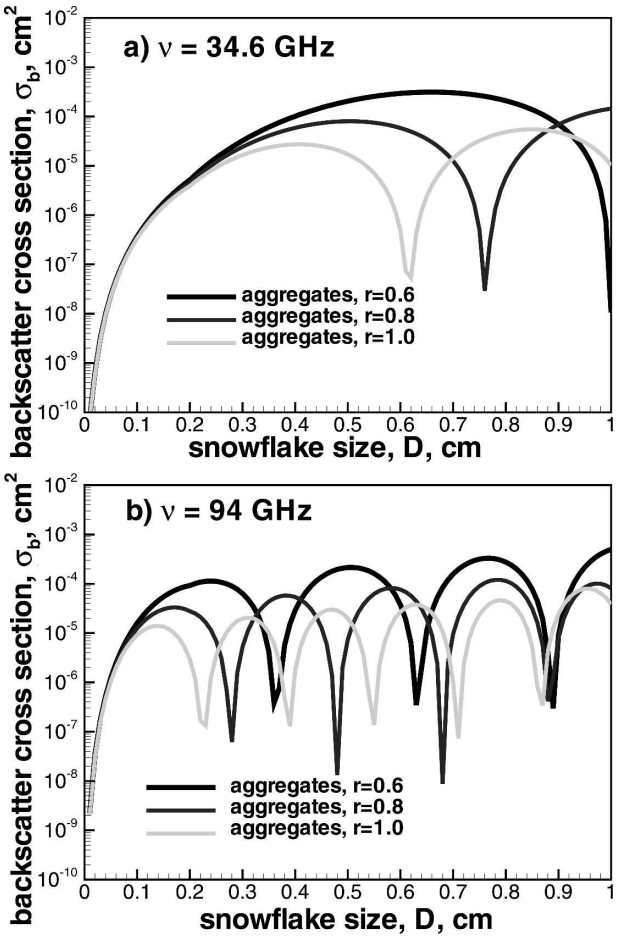

FIG. 1. Backscatter cross sections of horizontally oriented aggregate snowflakes with aspect ratios 0.6, 0.8, and 1.0 at vertical incidence and frequencies (a) 34.6 and (b) 94 GHz as a function of snowflake major dimension.

$$(m_s^2 - 1)(m_s^2 + 2)^{-1} \approx P_i(m_i^2 - 1)(m_i^2 + 2)^{-1}, \quad (9)$$

where m_i is the complex refractive index of solid ice adopted from Warren (1984).

Figure 1 shows backscatter cross sections, σ_b, of horizontally oriented aggregate snowflakes with aspect ratios that are in the range $0.6 \leq r \leq 1$ when viewed at vertical incidence. The mass of snowflakes was modeled according to (3) and was preserved as r was changing. This means that effective bulk densities are different for snowflakes with the same size but different aspect ratios. Though Mie-type backscatter oscillations are present for all considered aspect ratios, as can be seen from Fig. 1, backscatter cross sections of nonspherical snowflakes already begin to deviate noticeably from the spherical model already at major dimen-

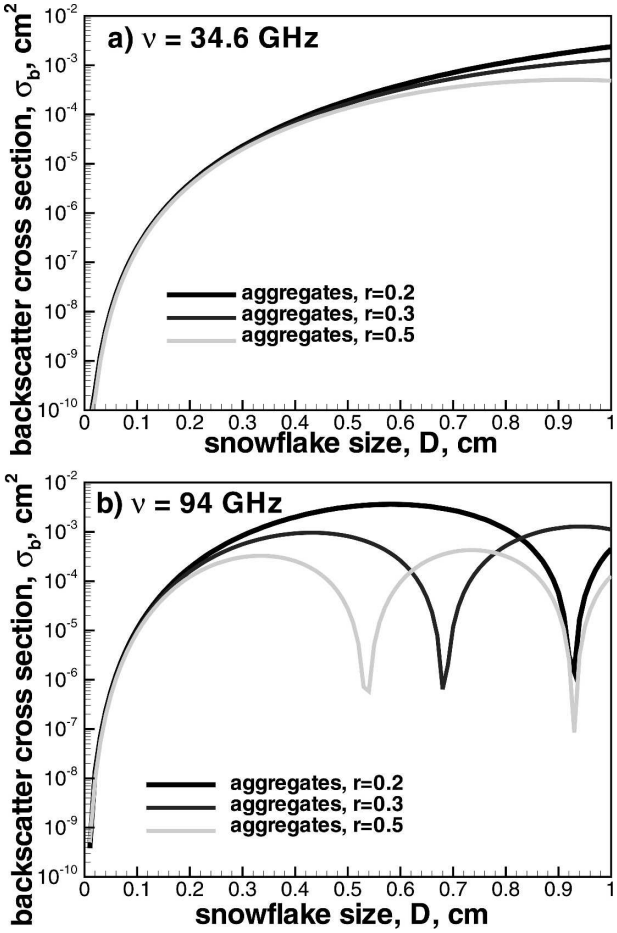

FIG. 2. As in Fig. 1 but for aspect ratios 0.2, 0.3, and 0.5.

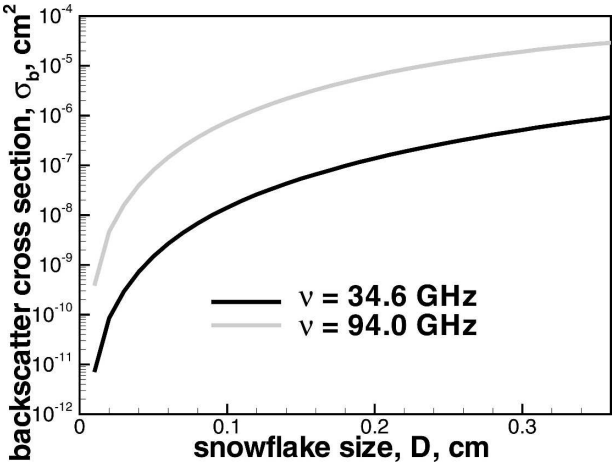

FIG. 3. Backscatter cross sections of horizontally oriented for dendritic crystals (P1d) as a function of crystal major dimension.

sions of about $D = 0.15$ cm for $\nu = 34.6$ GHz, and $D = 0.05$ cm for $\nu = 94$ GHz. This indicates that, for at least vertical-viewing geometry and millimeter radar wavelengths, the assumption that the backscatter cross section of an arbitrary snowflake would be the same as that of a sphere of ice having the same mass is not generally valid. This assumption, which is often used when calculating radar properties of snowflakes is, however, valid for lower radar frequencies in the Rayleigh scattering regime.

While, as mentioned above, $r \approx 0.6$ is expected to adequately describe natural snowflake aggregates, it is also instructive to examine backscatter cross sections for particles with smaller aspect ratios. Figure 2 presents results for $0.2 \leq r \leq 0.5$. Note that the T-matrix calculation routine often becomes unstable for particles with aspect ratios smaller than about 0.2, so no results are presented for $r < 0.2$. It can be seen from Fig. 2 that the dependence of backscatter cross sections σ_b on r becomes progressively less pronounced as r decreases. This is true especially for smaller particles.

Figure 3 shows backscatter cross sections for single pristine dendritic crystals (P1d) as a function of their size. Though the calculations presented in this figure were made for $r = 0.2$ they are expected also to be representative for smaller values of r because of the lesser sensitivity of σ_b to r at smaller values of aspect ratios and also because pristine crystals usually are smaller than aggregates and they are not expected to exceed a few millimeters in size. Note also that because the effective bulk density of snowflakes changes with their size, the results presented in Figs. 1–3 for one frequency cannot be obtained exactly from the results for the other frequency using simple frequency scaling.

4. Reflectivity of ensembles of snowflakes

a. Snowflake size distributions

Compared to the raindrop size distributions, information on snowflake size distributions (SSDs) in terms of real (not melted) snowflake dimensions is relatively scarce. However, different experimental and modeling studies (e.g., Braham 1990; Harimaya et al. 2000; Senn and Barthazy 2004) indicate that SSDs are generally exponential in shape down to a size of 1 mm, or even less. Since snowflakes with sizes greater than 1 mm typically dominate in both radar reflectivity and snowfall rate, the exponential model for snowflake number concentration in a form

$$N(D) = N_o \exp(-\Lambda D) \tag{10}$$

can be considered a reasonable modeling assumption.

One of the most complete experimental studies of snowflake size spectra in terms of snowflake real sizes

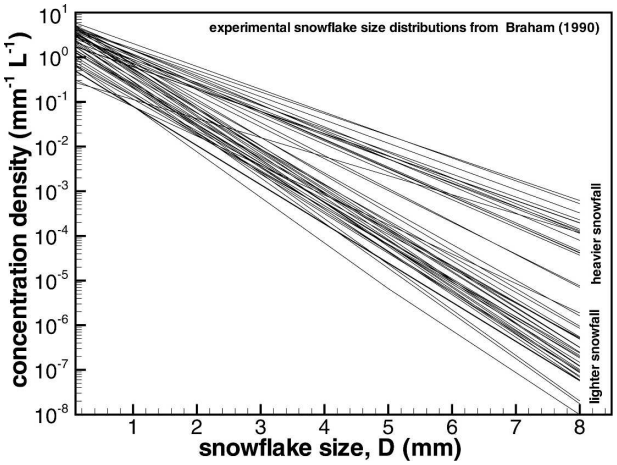

FIG. 4. Scatterplot of the intercept and slope parameters in experimental snowflake size distributions.

was presented by Braham (1990) who reported data that contained 49 experimental SSDs. Figure 4 shows these SSDs approximated by the exponential function with parameters N_o and Λ from Braham (1990). The majority of snowflakes in Braham's study appeared to be aggregate snowflakes with some amount of single spatial dendrites. Heavier snowfalls are characterized by smaller values of the parameter Λ. Later experimental studies (e.g., Harimaya et al. 2000) showed experimental SSD features similar to those reported by Braham (1990).

b. Z_e–S relations at millimeter wavelengths

Reflectivity of a snowflake ensemble is given by the integral

$$Z_e = \lambda^4 \pi^{-5} |(m^2 + 2)/(m^2 - 1)|^2 \int_{D_{\min}}^{D_{\max}} \langle \sigma_b \rangle N(D)\, dD, \tag{11}$$

where m is the complex refractive index of water at a given wavelength, λ, and the angular brackets in (11) indicate additional integrating over the snowflake orientations, which were assumed to be Gaussian with a 0° mean and SD = 9° as discussed in section 2b. Snowflake orientations in the azimuthal direction were assumed to be random, so for vertical incidence, Z_e does not depend on the polarization state of radar signals.

Liquid equivalent snowfall rate, S, can be expressed as

$$S = \rho_w^{-1} \int_{D_{\min}}^{D_{\max}} m(D) v_t(D) N(D)\, dD, \tag{12}$$

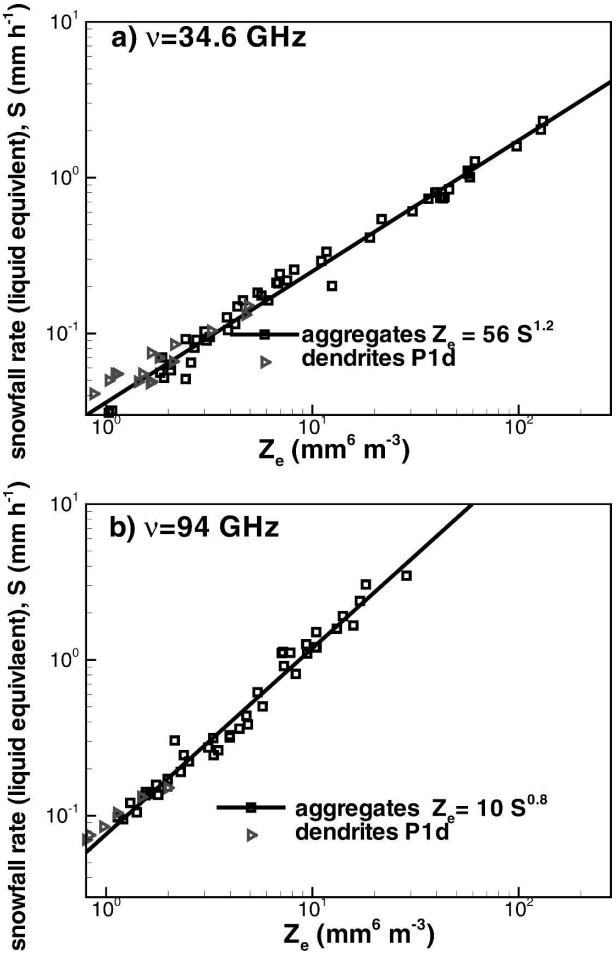

FIG. 5. Scatterplots of radar reflectivity at vertical incidence and snowfall rate at frequencies (a) 34.6 and (b) 94 GHz for experimental snowflake size distributions.

where ρ_w is the density of water, and the mass–size and fall velocity–size relations were discussed in sections 2c and 2d. The values of $D_{\min}$ and $D_{\max}$ in (10) and (11) were assumed to be 0.01 and 1 cm. This choice of $D_{\min}$ and $D_{\max}$ proved to be not very sensitive for the considered experimental SSDs. Modest variations of $D_{\min}$ and $D_{\max}$ (about 2%–20%) in the integral (12) did not result in significant changes in either Z_e or S.

Figure 5 shows the scatterplots of radar reflectivity versus liquid equivalent snowfall rate for frequencies 34.6 and 94 GHz calculated for the experimental SSDs with parameters from Fig. 4. Aggregate snowflake aspect ratio was assumed to be 0.6 and the mass and terminal fall velocities were calculated using (3) and (6). The best power-law fits drawn with Z_e as an independent variable for the aggregate snowflake assumption are $Z_e = 56S^{1.20}$ (34.6 GHz) and $Z_e = 10S^{0.8}$ (94 GHz), where Z_e in mm^6 m^{-3}and S in mm h^{-1}. Note that first the S–Z_e relations were developed considering Z_e

TABLE 1. Variability of Z_e–S (Z_e in mm^6 m^{-3}, S in mm h^{-1}) relations due to main assumptions about snowflake mass m, terminal fall velocity v_t, and aspect ratio r.

	Z_e–S relations for the aspect ratio $r = 0.6$, and (3), (6) used for m–D, v_t–D	Changing r $0.6 \rightarrow 0.8$	Increasing/decreasing m by 20%	Increasing/decreasing v_t by 20%
34.6 GHz	$Z_e = 56S^{1.2}$	$Z_e = 34S^{1.1}$	$Z_e = 66S^{1.2}/Z_e = 48S^{1.2}$	$Z_e = 46S^{1.2}/Z_e = 67S^{1.2}$
94 GHz	$Z_e = 10S^{0.8}$	$Z_e = 6S^{0.8}$	$Z_e = 13S^{0.8}/Z_e = 8S^{0.8}$	$Z_e = 8S^{0.8}/Z_e = 12S^{0.8}$

as an independent variable and then these relations were converted to the conventional Z_e–S form. The data scatter around the best-fit lines is rather modest. Due to stronger non-Rayleigh scattering effects, reflectivities at 94 GHz are significantly smaller than those at 34.6 GHz for the same values of snowfall rate S. The millimeter wavelength Z_e–S relations are quite different from those obtained by various researches for longer wavelength radars (Rasmussen et al. 2003).

While it is expected that aggregate snowflakes are the dominant hydrometeor type in appreciable snowfalls, for comparison reasons, calculations were also performed using the dendritic crystal model and the same experimental SSDs. The mass–size and fall velocity–size relations in this case are given by (5) and (7). The results for which dendrite reflectivities were greater than 0 dBZ are also shown in Fig. 5. For 34.6 GHz the aggregate best fit also rather well describes the dendrite data. It is not quite so for the 94-GHz data, although deviations of the dendrite data from the best power-law fit for aggregates are still not very significant. Reflectivities that are less than about 0 dBZ are more characteristic of nonprecipitating clouds and were not considered here.

c. *Variability of Z_e–S relations due to assumptions*

The main assumptions affecting radar reflectivity values, Z_e, include those about the particle mass and shape. While in the Rayleigh scattering regime, backscatter cross sections of individual particles are proportional to the square of particle masses, the resonance effects diminish the backscatter–mass dependence. The shape effects, which are not very pronounced for small particles, however, become progressively more important (especially for vertical incidence at horizontally oriented scatterers) as particles grow larger and transition to the sizes that are outside the Rayleigh scattering regime. The assumption about particle mass also affects the liquid equivalent snowfall rates, S. The values of S are also affected by the assumption about the terminal fall velocity–size relation.

The aggregate particle mass–size relation given by (3) and the terminal fall velocity–size relation given by (6) and an assumption about the $r = 0.6$ aspect ratio were used to produce the data presented in Fig. 5. Table 1 shows how the best fit power-law Z_e–S relations would vary if one of the main assumptions is changed. To assess this variability the particle mass and fall velocity were changed by 20% compared to values from Eqs. (3) and (6), respectively, and the particle aspect ratio was changed from 0.6 to 0.8. A more random orientation of snowflakes will be manifested similarly as an increase in r. These changes in the main assumptions may represent the reasonable uncertainties of corresponding assumptions. Indeed, the fall velocity approach of Mitchell and Heymsfield (2005), for example, provides fall velocities of 1 cm aggregates (which is a typical aggregated snowflake size) of about 1 m s^{-1}. The Khvorostyanov and Curry (2002) approach provides 1.4 m s^{-1} for the same particle size. This is about $\pm 20\%$ from their mean value of 1.2 m s^{-1}. Two different mass–size relations for aggregates from Mitchell (1996) provide similar percentage differences if applied to larger aggregate sizes.

It can be seen from Table 1 that there is an appreciable sensitivity of the Z_e–S relations to main assumptions. Assuming the independence of the assumption uncertainties, one can expect variability of at least a factor of 2 in the coefficients of the Z_e–S relations. Variability in the exponents of these relations is more modest, though it also contributes to the overall uncertainty in the correspondence between Z_e and S. It should be noted also that, compared to the low observational angles, the vertical radar beam observations (which is the most common configuration for K_a- and W-band radars) and the preferable orientation of snowflakes with their major dimension in the horizontal plane result in larger variability of backscatter due to changes in the particle aspect ratio.

5. Attenuation of radar signals in snowfall

Attenuation of radar signals at centimeter wavelengths in dry snowfall is very small and is usually neglected. The T-matrix approach used in this study to calculate backscatter properties of snowflakes was also

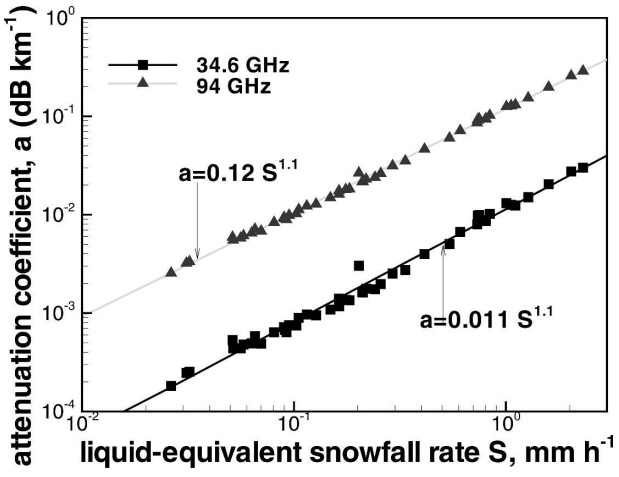

FIG. 6. Scatterplots of the attenuation coefficient at vertical incidence and snowfall rate for experimental snowflake size distributions.

used to estimate attenuation of K_a- and W-band signals in snowfall. The specific attenuation coefficient, a, can be obtained by integrating imaginary parts of the forward scattering amplitudes f:

$$a = 2\lambda \int_{D_{\min}}^{D_{\max}} \langle \mathrm{Im}[f(D)] \rangle N(D)\, dD, \qquad (13)$$

where the angular brackets are used, as before, to indicate additional integrating over the snowflake orientations. As was the case for reflectivity, there is no polarization dependence in the attenuation coefficient for the vertical incidence and mean snowflake orientation with major dimensions in the horizontal plane. The forward scattering amplitude f relates to the dimensionless amplitude matrix element S_o, which customarily is used in optics as

$$S_o = -2\pi i f \lambda^{-1}. \qquad (14)$$

Figure 6 shows scatterplots of the attenuation coefficients at −5°C versus liquid-equivalent snowfall rates at K_a- and W-band radar frequencies calculated for the assumed snowflake aspect ratio $r = 0.6$ and the same experimental SSDs that were used in reflectivity modeling. Complex refractive indices of solid ice corresponding to a temperature of −5°C are about $1.78 - i0.0024$ (34.6 GHz) and $1.78 - i0.0043$ (94 GHz).

The best-fit power law approximations for the data in Fig. 6 are $a = 0.011S^{1.1}$ and $a = 0.12S^{1.1}$ for 34.6 and 94 GHz, respectively. It can be seen that the dry snow attenuation at K_a band is fairly small and can be neglected for most practical cases. The attenuation at W band, however, is about one order of magnitude higher than that at K_a band and, probably, needs to be accounted for when measuring snowfall with higher precipitation rates in thick snow layers. The total attenuation in such cases can be appreciable and reach or even exceed 1 dB, which is on the order of a typical absolute calibration uncertainty of radars. For wet and/or rimed snow, attenuation can be significantly larger.

It should be noted also that the attenuation in the atmospheric gases (i.e., water vapor and oxygen) generally should be accounted for when interpreting measurements at W band at longer ranges (Stephens et al. 2002). Gases attenuation at K_a band at vertical incidence that typically amounts to fractions of 1 dB often can be neglected especially in dry cold atmospheres.

6. Summary and conclusions

Millimeter-wavelength radars operating at K_a and W bands are being increasingly used in the atmospheric remote sensing. These radars are typically employed either in a vertical-pointing mode (for ground based radars) or in a nadir-pointing mode (for airborne and spaceborne radars). A number of ground-based millimeter wavelength cloud profiling radars have been deployed in the colder climates and spaceborne radars are usually designed to operate at polar orbits, thus providing frequent coverage of high latitudes where snowfall is common. Although these radars' primary use is remote sensing of nonprecipitating clouds, they can also potentially be used for snowfall measurements. Adding quantitative snowfall information derived from radar measurements will be useful in many climate and cloud physics applications.

In this study, modeling of reflectivity–liquid-equivalent snowfall rate was performed for the common frequencies employed at K_a band (~35 GHz) and W band (~94 GHz). "Dry" snowfall, which is characterized by negligible amounts of liquid water in snow and snowflake riming, was studied. Nonspherical aggregate and single crystal dendritic snowflake models were used for calculations. These models included realistic mass–size and terminal fall velocity–size relations and assumed some flutter around the preferred orientation of snowflakes with their maximum dimensions in the horizontal plane. Experimental size distributions describing real (not melted) snowflake sizes were employed in this study.

Most common aggregate snowflake sizes are already outside the Rayleigh scattering regime at K_a- and especially at W-band frequencies. For vertical/nadir-pointing geometry, backscatter properties of snow-

flakes noticeably depend on snowflake overall shape (i.e., aspect ratio). The typical radar reflectivity–snowfall rate relations for aggregate snowflakes calculated for a set of basic assumptions (see Table 1) are $Z_e = 56^{1.20}$ (34.6 GHz) and $Z_e = 10S^{0.8}$ (94 GHz). These relations are generally valid also for snowfall consisting of single dendrite crystals (P1d), though snowfall rates and thus accumulations of such snowfalls are usually significantly less compared to the snowfalls consisting of aggregates. Though these relations were developed for "dry" snowfall, they are expected to be applicable for snowfall with some light degree of riming. Dry snow typically forms at colder temperatures (usually less than about -12°C) and is characterized by mean vertical Doppler velocities that are less than about 1.2–1.4 m s^{-1}. A significant increase in snowflake riming and/or wetness is likely to cause changes in Z_e–S relations.

The strong non-Rayleigh behavior of backscatter at millimeter wavelengths in K_a and W bands results in reflectivity being proportional to the lower moment of the snowflake size distribution. As a result the exponents in the Z_e–S relations are closer to unity compared to the longer wavelength radars. The proportionality of Z_e and S to similar moments of the size distribution can, in part, explain small data scatter in Fig. 5. For precipitation radar frequencies (3–10 GHz), both coefficients and exponents in Z_e–S relations are larger. Typically for such frequencies, coefficients vary from 50 to 400 while the exponents vary between 1.5 and 2 (e.g., Rasmussen et al. 2003).

Uncertainties in the coefficients of Z_e–S relations caused by variability in the snowflake shape, and in the parameters of mass–size and terminal fall velocity–size relations are rather substantial. These coefficient uncertainties can easily be as high as a factor of ~2; thus, the errors in the snowfall rate and accumulation estimations for radar reflectivity measurements could be appreciable. These errors can potentially be reduced if the coefficient tuning is performed based on collocated radar and snow gauge measurements. Such a tuning approach is often used in rainfall measurements when parameters of standard Z_e–R (R here is rainfall rate) relations are adjusted based on the rain gauge measurements that are deployed in the radar coverage area. There are, however, no high quality collocated datasets for millimeter-wavelength radars and snow gauge data available at the moment, so this direction for refinement of Z_e–S relations should be left for further studies.

Acknowledgments. This research was supported by the Office of Science (Biological and Environmental Research), U.S. Department of Energy, Grant DE-FG02-05ER63954, and the CloudSat project.

REFERENCES

Aydin, K., and J. Singh, 2004: Cloud ice crystal classification using a 95-GHz polarimetric radar. *J. Atmos. Oceanic Technol.,* **21,** 1679–1688.

Barber, P., and C. Yeh, 1975: Scattering of electromagnetic waves by arbitrarily shaped dielectric bodies. *Appl. Opt.,* **14,** 2864–2872.

Battan, L. J., 1973: *Radar Observation of the Atmosphere*. University of Chicago Press, 324 pp.

Braham, R. R., Jr., 1990: Snow particle size spectra in lake effect snows. *J. Appl. Meteor.,* **29,** 200–207.

Brown, P. R. A., and P. N. Francis, 1995: Improved measurements of the ice water content in cirrus using a total-water probe. *J. Atmos. Oceanic Technol.,* **12,** 410–414.

Dungey, C. E., and C. F. Bohren, 1993: Backscattering by nonspherical hydrometeors as calculated by the coupled-dipole method: An application in radar meteorology. *J. Atmos. Oceanic Technol.,* **10,** 526–532.

Harimaya, T., H. Ishida, and K. Muramoto, 2000: Characteristics of snowflake size distributions connected with the difference of formation mechanism. *J. Meteor. Soc. Japan,* **78,** 233–239.

Heymsfield, A. J., 1972: Ice crystal terminal velocities. *J. Atmos. Sci.,* **29,** 1348–1357.

——, A. Bansemer, C. Schmitt, C. Twohy, and M. R. Poellot, 2004: Effective ice particle densities derived from aircraft data. *J. Atmos. Sci.,* **61,** 982–1003.

Hunter, S. M., and E. W. Holroyd, 2002: Demonstration of improved operational water resources management through use of better snow water equivalent information. Bureau of Reclamation Rep. R-02-02, U.S. Department of the Interior, 75 pp.

Khvorostyanov, V. I., and J. A. Curry, 2002: Terminal velocities of droplets and crystals: Power laws with continuous parameters over the size spectrum. *J. Atmos. Sci.,* **59,** 1872–1884.

Korolev, A., and G. Isaac, 2003: Roundness and aspect ratio of particles in ice clouds. *J. Atmos. Sci.,* **60,** 1795–1808.

Lemke, H. M., and M. Quante, 1999: Backscatter characteristics of nonspherical ice crystals: Assessing the potential for polarimetric radar measurements. *J. Geophys. Res.,* **104,** 31 739–31 752.

Liao, L., R. Meneghini, T. Iguchi, and A. Detwiler, 2005: Use of dual-wavelength radar for snow parameter estimates. *J. Atmos. Oceanic Technol.,* **22,** 1494–1506.

Locatelli, J. D., and P. Hobbs, 1974: Fall speeds and masses of solid precipitation particles. *J. Geophys. Res.,* **79,** 2185–2197.

Magono, C., and T. Nakamura, 1965: Aerodynamic studies of falling snowflakes. *J. Meteor. Soc. Japan,* **43,** 139–147.

——, and C. W. Lee, 1966: Meteorological classification of natural snow crystals. *J. Fac. Sci., Hokkaido Univ., Ser. 2,* **7,** 321-335.

Matrosov, S. Y., 1992: Radar reflectivity of snowfall. *IEEE Trans. Geosci. Remote Sens.,* **30,** 454–461.

——, 1993: Possibilities of cirrus particle sizing from dual-frequency radar measurements. *J. Geophys. Res.,* **98,** 20 675–20 684.

——, 1998: A dual-wavelength radar method to measure snowfall rate. *J. Appl. Meteor.,* **37,** 1510–1521.

——, R. F. Reinking, R. A. Kropfli, and B. W. Bartram, 1996: Estimation of ice hydrometeor types and shapes from radar polarization measurements. *J. Atmos. Oceanic Technol.,* **13,** 85–96.

——, ——, ——, B. E. Martner, and B. W. Bartram, 2001: On the

use of radar depolarization ratios for estimating shapes of ice hydrometeors in winter clouds. *J. Appl. Meteor.,* **40,** 479–490.

——, A. J. Heymsfield, and Z. Wang, 2005a: Dual-frequency radar ratio of nonspherical atmospheric hydrometeors. *Geophys. Res. Lett.,* **32,** L13816, doi:10.1029/2005GL023210.

——, R. F. Reinking, and I. V. Djalalova, 2005b: Inferring fall attitudes of pristine dendritic crystals from polarimetric radar data. *J. Atmos. Sci.,* **62,** 241–250.

Mitchell, D. L., 1988: Evolution of snow-size spectra in cyclonic storms. Part I: Snow growth by vapor deposition and aggregation. *J. Atmos. Sci.,* **45,** 3431–3451.

——, 1996: Use of mass- and area-dimensional power laws for determining precipitation particle terminal velocities. *J. Atmos. Sci.,* **53,** 1710–1723.

——, and A. J. Heymsfield, 2005: Refinements in the treatment of ice particle terminal velocities, highlighting aggregates. *J. Atmos. Sci.,* **62,** 1637–1644.

Oguchi, T., 1983: Electromagnetic wave propagation and scattering in rain and other hydrometeors. *Proc. IEEE,* **71,** 1029–1078.

Pruppacher, H. R., and J. D. Klett, 1997: *Microphysics of Clouds and Precipitation*. Kluwer Academic, 954 pp.

Rasmussen, R., M. Dixon, S. Vasiloff, F. Hage, S. Knight, J. Vivekanandan, and M. Xu, 2003: Snow nowcasting using a real-time correlation of radar reflectivity with snow gauge accumulation. *J. Appl. Meteor.,* **42,** 20–36.

Schneider, T. L., and G. L. Stephens, 1995: Theoretical aspects of modeling backscattering by cirrus ice particles at millimeter wavelengths. *J. Atmos. Sci.,* **52,** 4367–4385.

Sekhon, R. S., and R. C. Srivastava, 1970: Snow size spectra and radar reflectivity. *J. Atmos. Sci.,* **27,** 299–307.

Senn, P., and E. Barthazy, 2004: In-situ observations and modeling of aggregation of snowfall. *Proc. European Conf. on Radar Meteorology* (ERAD-2004), Visby, Sweden, Copernicus GmbH, 253–256.

Stephens, G. L., and Coauthors, 2002: The CloudSat mission and the A-train. *Bull. Amer. Meteor. Soc.,* **83,** 1771–1790.

Super, A. B., and E. W. Holroyd, 1998: Snow accumulation algorithm for the WSR-88D radar: Final report. Bureau of Reclamation Rep. R-98-5, U.S. Department of the Interior, 75 pp.

Wang, Z., G. M. Heymsfield, L. Li, and A. J. Heymsfield, 2005: Retrieving optically thick ice cloud microphysical properties by using airborne dual-wavelength radar measurements. *J. Geophys. Res.,* **110,** D19201, doi:10.1029/2005JD005969.

Warren, S. G., 1984: Optical constants of ice from the ultraviolet to the microwave. *Appl. Opt.,* **23,** 1206–1225.